

Ω_{bar} in NGC 5597 from VLA H I 21 cm Observations

J. ANTONIO GARCIA-BARRETO¹ AND EMMANUEL MOMJIAN²

¹*Instituto de Astronomia, Universidad Nacional Autónoma de México,
Apartado Postal 70-264, Ciudad de México 04150, México*

²*National Radio Astronomy Observatory, P. V. D. Science Operations Center,
P.O. Box 0, 1003 Lopezville Road, Socorro, 87801, New Mexico, U.S.A.*

(Accepted June 7, 2022)

ABSTRACT

We report Very Large Array B-configuration observations of the atomic hydrogen 21 cm line emission from the barred disk galaxy NGC 5597 at an angular resolution of $\sim 7''.1 \times 4''.2$. Using the resonance method, and assuming the ratio of the corotation radius to the semi-major axis of the stellar bar is unity ($\mathcal{R} \equiv R_{\text{CR}}/a_{\text{bar}} = 1$), we estimate the angular pattern speed of the stellar bar to be, $\Omega_{\text{bar}} \sim 15.3 \text{ km s}^{-1} \text{ kpc}^{-1}$. This constant value for Ω_{bar} crosses $\Omega_{\text{gas}} + \kappa(R)/4$ at a distance $\sim 6.73 \text{ kpc}$ which would correspond to the spatial location of the north spiral structure near an outer $m=4$ resonance. This value of Ω_{bar} is similar to the values estimated for other bright nearby barred galaxies that exhibit circumnuclear rings (near ILR) or outer rings (near OLR).

Keywords: galaxies: active: individual (NGC 5597) — galaxies: kinematics and dynamics — galaxies: ISM — galaxies: spiral

1. INTRODUCTION

There is growing evidence for the existence of weak nuclear activity in normal disk galaxies, with and without a prominent stellar bar, supported by observational detections of nuclear H α low velocity bipolar outflows, e.g., M81 Sb(r)I-II (Goad 1976), NGC 1068 Sb(rs)II (Ulvestad, Neff & Wilson 1987) which was more recently reported to host a stellar bar (Scoville et al. 1988b), M51 Sbc(s)I-II (Ford et al. 1985; Cecil 1988; Crane & van der Hulst 1992; Scoville et al. 1998), NGC 3079 Sc pec: (Veilleux et al. 1994), M101 Sc(s)I (Moody et al. 1995), NGC 3367 SBC(s)II (Garcia-Barreto et al. 1998, 2002), and NGC 1415 SBA late (Garcia-Barreto et al. 2019). This suggests that such galaxies represent a low end of scale for nuclear activity after quasars, BL Lac objects, radio galaxies, and Seyfert galaxies. Such weak nuclear activity in normal disk galaxies originates around central massive black holes ($M_{\text{BH}} \sim \text{a few } 10^6 M_{\odot}$), with the level of the activity being governed by the gas supply to fuel these central

engines (Norman & Silk 1983). An open question in the case of barred galaxies is whether there is a correlation among the onset of nuclear activity, their central gas, and the angular velocity pattern of their stellar bar.

Stellar bars¹ represent a small non-axisymmetrical gravitational potential Φ_{bar} compared to the axisymmetric gravitational potential of a disk galaxy Φ_{disk} .

NGC 5597, located in the Southern Virgo - Libra Cloud of Galaxies, is one such nearby galaxy with a prominent stellar bar. It is a bright ($m_B \sim 12.57$) disk galaxy classified as SBC(s) II (Sandage & Tammann 1987) and as SAB(s)cd in NED². It forms a gravitationally bound isolated pair with the disk galaxy NGC 5595 (Sc).

NGC 5597 is one of our original set of 56 bright and nearby Shapley-Ames barred galaxies with IRAS colors that suggest central massive star formation. Their

¹ Sustained by stars in x_1 orbits that lie along the major axis of the bar (Contopoulos 1980; Contopoulos & Papayannopoulos 1980)

² The NASA/IPAC Extragalactic Database (NED) is operated by the Jet Propulsion Laboratory, California Institute of Technology, under contract with the National Aeronautics and Space Administration.

2D optical images in the red continuum filter I (8040 Å) and in the H α +N II narrow line filter have been published by Garcia-Barreto et al. (1996). The IRAS 60 μ m and 100 μ m flux densities of NGC 5597 are 8.7 Jy and 15.32 Jy, respectively, with a dust temperature of $T_{\text{dust}} \sim 36$ K. The (IRAS) far-IR luminosity is $L_{\text{FIR}} \sim 2.2 \times 10^{10} L_{\odot}$ (Garcia-Barreto et al. 1996).

In this paper, we present Karl G. Jansky Very Large Array (VLA) observations of the atomic hydrogen, H I 21 cm, gas emission from the barred disk galaxy NGC 5597 to determine its two dimensional gas velocity field and estimate its bar’s angular pattern speed, Ω_{bar} . For this measurement, we utilize the resonance method that has been proven to be a valid technique to apply on nearby bright barred galaxies with rings near the Inner Lindblad Resonance (ILR) or Outer Lindblad Resonance (OLR). The outline of this paper is as follows: Section 2 presents the observations, data reduction, and analysis, Section 3 reports the results and discussion, and Section 4 presents the summary and conclusions.

2. OBSERVATIONS AND DATA REDUCTION

The observations to image the H I 21 cm emission from the barred disk galaxy NGC 5597, and map its two dimensional velocity field, were carried out with the VLA of the NRAO³ in its B-configuration (maximum baseline $b_{\text{max}} = 11.1$ km) on 2019 June 6, 7, 11, 16, 18, & 22.

Each of the six observing sessions had a duration of 1.67 hr (100 min on-source time). The L-band receiver of the VLA was tuned to the redshifted frequency of the H I 21 cm line ($\nu_{\text{rest}} = 1420.405752$ MHz) at a heliocentric velocity⁴ corresponding to $V = 2700$ km s^{−1}. (All velocities in this paper are heliocentric, using the optical convention for redshift.) The Wideband Interferometric Digital ARchitecture (WIDAR) correlator of the VLA was set to deliver a single 4 MHz subband with 256 spectral channels ($\Delta\nu_{\text{channel}} = 15.625$ kHz), covering a velocity range of $\Delta V \sim 843$ km s^{−1}. This velocity span is sufficient to cover the full width at zero intensity of the H I 21 cm emission line from NGC 5597, and provide line-free channels on both sides of the H I emission for continuum subtraction. In addition to the target field, we observed the source 3C 286 as the flux density scale and bandpass calibrator, and J1448-1620 as the complex gain calibrator. A more detailed description of

the system setup will be provided in a forthcoming paper on the H I 21 cm kinematics and dynamics of both NGC 5595 and NGC 5597 (Garcia-Barreto & Momjian 2022, in preparation).

We utilized both the Common Astronomy Software Applications (CASA) and the Astronomical Image Processing System (AIPS) packages of the NRAO for data reduction and analysis. The initial calibration steps, e.g., bandpass, flux density scale, complex gain calibration, continuum subtraction, and imaging, were performed in CASA. All the spectral and kinematics analysis were carried out in AIPS.

Image cubes from each of the six observing sessions were made and examined to determine the H I line and the line-free channels. Then the continuum emission was subtracted in the uv plane. The final image cube using the combined uv data of all the sessions was produced with a cell size of 1''0, and Briggs weighing with robust parameter value of 0.8 in CASA, resulting in a synthesized beam size, at full width half maximum (FWHM), of $\sim 7''.1 \times 4''.2$ (P.A. $\sim -10^\circ$). This angular resolution corresponds to a linear resolution of $\sim 1.33 \times 0.78$ kpc². The final H I image cube was imported to AIPS for further analysis. In there Moments 0, 1, and 2 were made using a flux density cutoff of 2.5σ , with $1\sigma \sim 450 \mu\text{Jy beam}^{-1} \text{ channel}^{-1}$.

3. RESULTS AND DISCUSSION

3.1. NGC 5597: an SBc disk galaxy

The disk galaxies NGC 5595 and NGC 5597 are in the Southern Virgo - Libra Cloud of galaxies, Tully’s group 41-14(+14), with a very low galaxy volume density of only 0.16 galaxies Mpc^{−3}; see their spatial location at the galactic coordinates $l^{\text{II}} \sim 332^\circ 8$, $b^{\text{II}} \sim +40^\circ 7$ in Plates 1 and 5 in Tully & Fischer (1987), and in α and δ in Fig. 2 of Tammann (1985). Since these two galaxies are separated by $\Delta\alpha \sim 13^s 54$, $\Delta\delta \sim 138''$, or about 3'.97 on the plane of the sky while having similar systemic velocities (see Table 1), we may confidently say that they form a physically isolated and gravitationally bound pair of disk galaxies. Therefore, in this paper, we adopt a Hubble spectroscopic distance of $D_{\text{pair}} = 38.6$ Mpc (Tully 1988) giving an angular-to-linear scale conversion of $1'' = 187.14$ pc.

Figure 1 shows a reproduction of the optical blue continuum 103aO emission from the pair of disk galaxies NGC 5597 (south-east) and NGC 5595 (north-west) in grey scale (relative units) taken with the OAN-SPM 2.1 m optical telescope in Mexico (Diaz-Hernández et al. 2009). In this blue optical con-

³ The National Radio Astronomy Observatory is a facility of the National Science Foundation operated under cooperative agreement by Associated Universities, Inc.

⁴ NGC 5597 was observed simultaneously with the nearby galaxy NGC 5595 using a single pointing midway between the two sources. They have very comparable recession velocities of ~ 2700 km s^{−1}

Table 1. NGC 5597: Coordinates, Hubble type, Distance, Systemic H I Velocity

Galaxy	$\alpha(\text{J2000})$	$\delta(\text{J2000})$	Ref.	RSA type	NED type	Distance	Ref.	$V(\text{H I})_{\text{sys}}$	Ref.
Name	<i>hh mm ss</i>	$^{\circ} \text{ } ^{\circ} \text{ } ''$				Mpc		km s^{-1}	
(11)	(12)	(13)	(14)	(15)	(16)	(17)	(18)	(19)	(20)
NGC 5595	14 24 13.3	−16 43 21.6	1	Sc(s) II	SAB(rs)c	38.6	2	2697	3
NGC 5597	14 24 27.49	−16 45 45.9	1	SBC(s) II	SAB(rs)b	38.6	2	2698	3

NOTE—1) (Díaz-Hernández et al. 2009), 2) (Tully 1988), 3) (Paturel et al. 2003)

tinuum image, there are no bridges or structures connecting the two galaxies. Figure 2 shows a reproduction of the optical red, filter I 8040 Å, continuum image of NGC 5597 convolved with a Gaussian beam of $\sim 1''.5 \times 1''.5$ at FWHM (García-Barreto et al. 1996). The grey scale and the contours in this figure are also in relative units. Both the blue and red optical continuum images of NGC 5597 show a central elongated structure extending about $2a \sim 28''.3$ by $2b \sim 14''$ at a P.A. $\sim 52^{\circ}$. We will refer to this structure as the stellar boxy bar of NGC 5597 (see the south-east galaxy, NGC 5597, in Figure 1, and its more detailed view in Figure 2).

Additionally, in Figure 1, and more specifically in Figure 2, there are at least four narrow and curved structures as spiral arms outside the central region in NGC 5597 (labeled 1 to 4 in Figure 2). From the optical red continuum image, the first structure (1) starts from the NE half of the boxy stellar bar and extends to the SE, the second structure (2) starts from the SW of the southern half of the boxy bar and extends further to the SW, the third structure (3) starts from the NW of the southern half of the boxy bar and extends further NW joining the outer fourth structure. The fourth structure (4) seems to start from the SW of the disk and continues counter clockwise to N, NE, and SE just parallel on the outside of the first structure.

3.1.1. Estimation of Stellar Bar in NGC 5597

In general, the estimation or the determination of the size of a stellar bar, even for nearby bright disk galaxies, has been a challenging topic for not only observational studies, but also for image analysis as well as computer simulations (Erwin 2005). From the observational perspective, some of the reasons are: the wavelength of the continuum images – optical blue, red, IR, MIR –, inclusion of the bulge, subtraction of intensity from the bulge, and the no-agreed-upon method –the projected semimajor axis of the stellar bar on the plane of the sky, the

projected semimajor axis of the stellar bar on the kinematical semimajor axis of the disk galaxy, and the radius where the intensity along the stellar bar has fallen to half of its peak value. From the computer image analysis perspective, some of the reasons are: the different and elegant mathematical algorithms – ellipse fitting, fourier transform $m=2$ amplitudes, modified Ferrer profiles, and Lagrangian radius, and from the computer N-body simulations perspective: the angular momentum transfer, gas viscosity, galaxy harassments, galaxy close-by interactions, (Kormendy 1979; Kent 1990; Contopoulos 1980; Contopoulos & Papayannopoulos 1980; Quillen et al. 1994; Martin 1995; Debattista & Sellwood 2000; Athanassoula & Misiriotis 2002; Athanassoula 2003; Erwin 2005; Salo et al. 2015; Díaz-García et al. 2016).

Kormendy (1977, 1979, 1983) did extensive work in modeling different independent stellar components in galaxy brightness profiles. For instance, he identified the most fundamental components to be: spherical central bulge, exponential axisymmetric disk, and bar, and as secondary components: lens, ring, outer ring, and outer lens. He also concluded that the total mass of a disk galaxy does not determine whether the galaxy makes a bar, but if it does make one, the total mass uniquely determines the size of the bar (Kormendy 1979). Kent & Glauddell (1989) and Kent (1990) also made detailed photometry of two barred galaxies, NGC 936 and NGC 4596, with analytic mathematical expressions to the luminosity profiles of each component (bulge, bar, and disk) to construct bar models. They did give two values for a_{bar} for each galaxy: i) on the plane of the sky and ii) projected on the major axis of the disk. In particular, a_{bar} in NGC 4596 was reported to be the radius where the intensity along the major axis of the bar has fallen to half of its peak value (Kent 1990).

For NGC 5597, previous estimation of its stellar bar’s semi-major axis by the same group of astronomers has

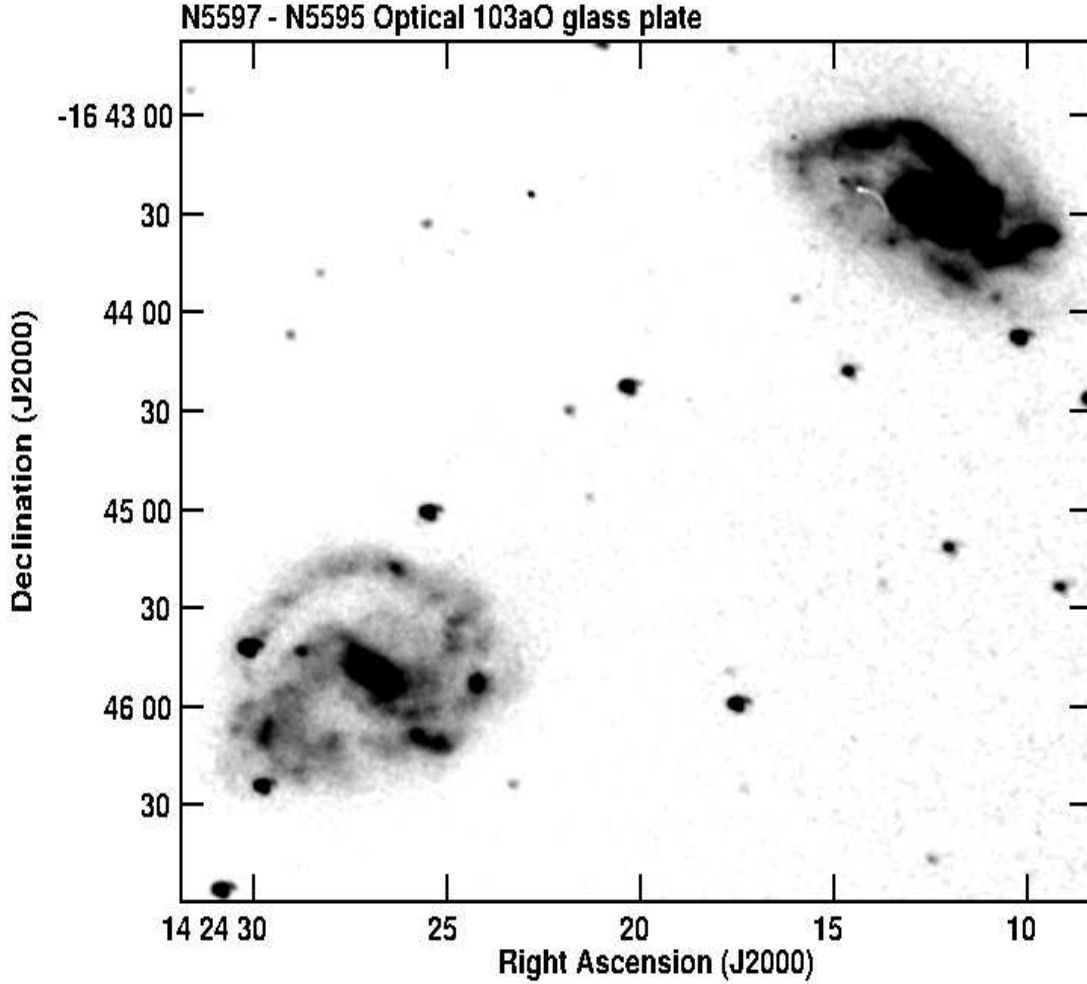


Figure 1. Reproduction of the optical blue continuum image (glass plate 103aO) of the close-pair disk galaxies NGC 5597 at the south east and NGC 5595 at the north west, obtained with the OAN-SPM 2.1 m optical telescope in Mexico (Díaz-Hernández et al. 2009). The flux density scale is not calibrated. Grey scale is from $2 \rightarrow 27.8\sigma$, where σ is the noise in arbitrary units.

been published with surprisingly two different values, namely, $a_{\text{bar}} \sim 3''.79$ (Díaz-García et al. 2016), and $a_{\text{bar}} \sim 6''.51$ (Salo et al. 2015)⁵.

Figures 3 and 4 (left panels) show the innermost regions of the blue (103aO) and red (8040 Å) images, extracted from Figures 1 and 2, to provide a more detailed view of the elongated stellar structure in NGC 5597, notice the lack of dust lanes in both images. The right panels in Figures 3 and 4 show the 1-D slice with intensity versus angular distance along P.A. $\sim 52^\circ$ EofN. Notice the exponential profile in the slice of the red image (Fig-

ure 4). The full width at half maximum intensity of the blue and red image profiles are $\text{FWHM}_{\text{blue}} \sim 10''.3$ and $\text{FWHM}_{\text{red}} \sim 5''.1$, respectively.

In addition to the two different values reported by Salo et al. (2015) and Díaz-García et al. (2016), the left panels of Figures 3 and 4 further demonstrate the challenge of deriving a reliable value for the semimajor axis of the stellar bar in NGC 5597. Here, clearly the optical red elongated structure shown by the boxy isophotal contours results in a semimajor axis value for the bar that is larger than those previously published.

In this paper, we used the more modest visual method analyzing the optical blue (103aO) images shown in Figures 1 and 3 and the optical red (broad band filter I 8040 Å) image shown in Figures 2 and 4 to estimate the semimajor axis of the stellar bar in NGC 5597. In particular, we determined the projected length, on the

⁵ Salo et al. 2015 from 3.6 μm S⁴G imaging, used a modified Ferrers profile to characterize bars, while Díaz-García et al. 2016 from the same 3.6 μm S⁴G imaging used i) maximum of the tangential to radial force, ii) $m=2$ Fourier density amplitude and iii) isophotal ellipticity, to characterize bars.

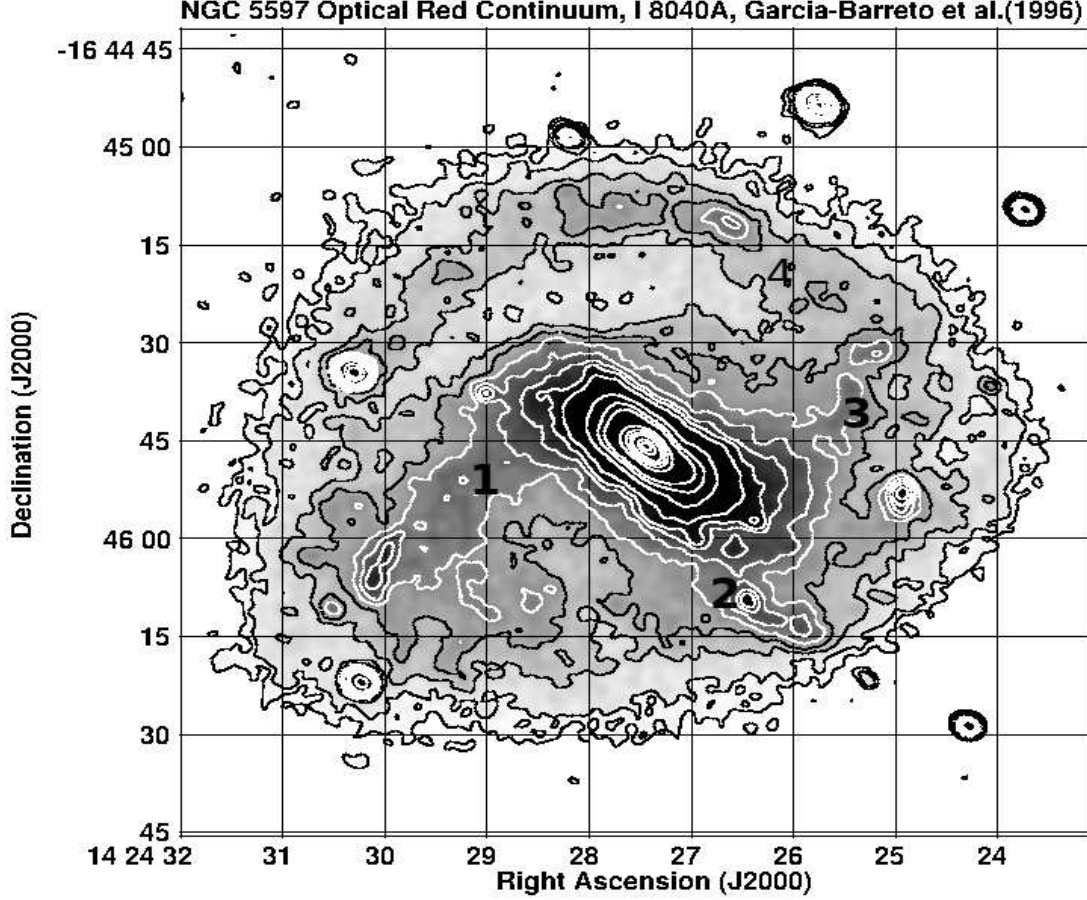


Figure 2. Reproduction of the optical red, filter I 8040 Å, continuum image that has been convolved with a Gaussian beam FWHM $\sim 1''.5 \times 1''.5$ in grey scale and in contours (Garcia-Barreto et al. 1996). The image had not been calibrated in intensity scale, thus the grey-scale stretch is in relative units proportional to noise from 5σ up to 37.7σ , where $1\sigma = 45$ in arbitrary units. Contours are 5, 7, 11, 15, 20, 25, 30, 34, 40, 60, 80, 100, 200, 300, 400, 500, 750, 900 $\times 1\sigma$. Note the boxy isophotes at radii larger than $5''.0$ that delineate a structure straddling the nucleus elongated in P.A. $\sim 52^\circ$ EofN.

plane of the sky, of the semimajor axis of the stellar bar, a_{bar} , that is, the distance from the nucleus (or photometric center) to the isophote still showing an elliptical boxy shape, just before the next isophote that deviates into azimuthally extended structures in the blue and red images. For this, we measured the distance from the center to north-east and from the center to south-west, and took the average of the two values for both blue and red images. The estimated a_{bar} values differ for the blue and red images, as expected, because the associated emission trace different stars; although the OB stars are brighter, the GK stars outnumber them (Mihalas & Binney 1981). The mean $a_{\text{bar}}^{\text{blue}} \sim 7''$, while the mean $a_{\text{bar}}^{\text{red}} \sim 14''$. Curiously $a_{\text{bar}}^{\text{blue}}$ roughly agrees with Salo et al. (2015) value of $a_{\text{bar}}^{\text{salo}} \sim 6''.51$. Further-

more, for the stellar bar in NGC 5597 (with no mass distribution model), we have estimated the radius where the intensity along its major axis falls to half of its peak value for both the blue and red images: $a_{\text{bar}}^{0.5b} \sim 5''.1$, and $a_{\text{bar}}^{0.5r} \sim 2''.5$.

At this point, we have six different estimates for the semimajor axis of the stellar bar in NGC 5597 *on the plane of the sky*, $a_{\text{bar}}^{\text{diaz}} \sim 3''.79$, $a_{\text{bar}}^{\text{salo}} \sim 6''.51$, $a_{\text{bar}}^{\text{blue}} \sim 7''$, and $a_{\text{bar}}^{\text{red}} \sim 14''$, $a_{\text{bar}}^{0.5b} \sim 5''.1$, and $a_{\text{bar}}^{0.5r} \sim 2''.5$.

Now, we will estimate the six different semimajor axis values of the stellar bar in NGC 5597 *projected on the kinematical major axis*, hereafter *ma*, from the value *on the plane of the sky*, hereafter *pls*, utilizing the mathematical expression $a_{\text{bar}}^{\text{ma}} = a_{\text{bar}}^{\text{pls}} \times \sqrt{\cos^2(\phi) + (\sin^2(\phi)/\sin^2(i))}$ (Kormendy 1983), where

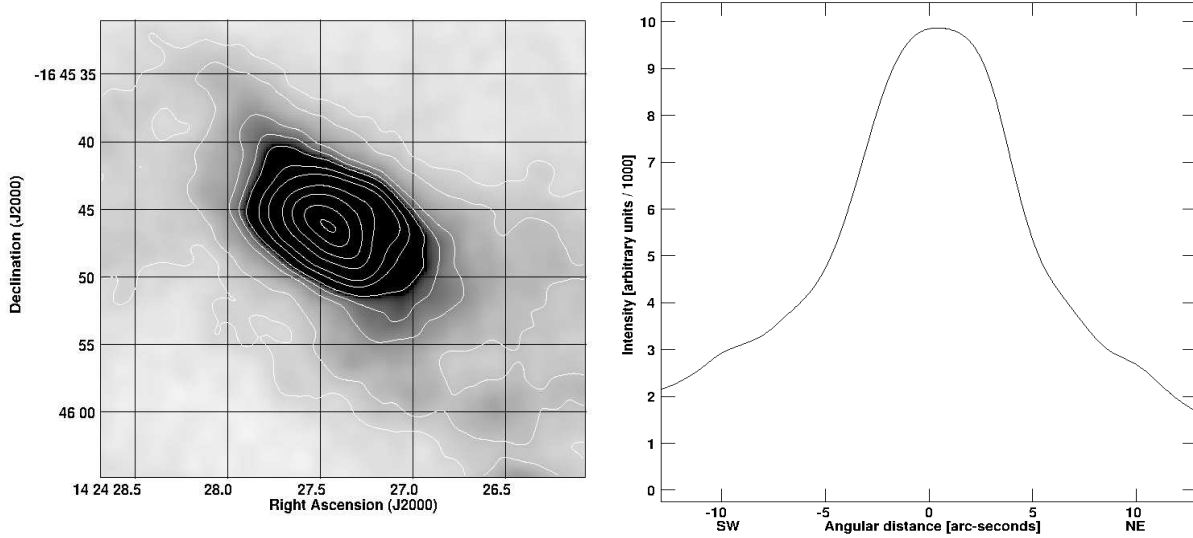


Figure 3. Left panel: innermost optical blue, 103aO, continuum image of the stellar bar in NGC 5597 in grey scale and in contours, extracted from Figure 1 (Díaz-Hernández et al. 2009). The image had not been calibrated in intensity scale, thus the grey-scale stretch is in relative units proportional to noise from 1.5σ to 39σ , where $1\sigma = 90$ in arbitrary units, and the contours are at 15, 20, 30, 35, 40, 50, 60, 80, 95, 107, $111.5 \times 1\sigma$, showing the extent of the boxy isophotal contours before a contour with azimuthal extensions. Boxy isophotes delineate a structure straddling the nucleus elongated in P.A. $\sim 52^\circ$ EofN. Right panel: one dimensional slice with intensity versus angular distance at P.A. $\sim 52^\circ$ EofN. Notice the lack of dust lanes.

ϕ is the angle difference between the P.A. of the kinematical semimajor axis of the disk galaxy and the P.A. of the semimajor axis of the stellar bar, and i is the inclination of the disk of the galaxy with respect to the plane of the sky. For NGC 5597, these angles are $\phi \sim 48^\circ$ and $i \sim 36^\circ$.

Thus, the six different values for the semimajor axis of the stellar bar in NGC 5597 *projected on the kinematical major axis* are: $a_{\text{bar}}^{d-ma} \sim 5''.42$, $a_{\text{bar}}^{s-ma} \sim 9''.31$, $a_{\text{bar}}^{\text{blue-ma}} \sim 10''$, and $a_{\text{bar}}^{\text{red-ma}} \sim 20''$, $a_{\text{bar}}^{0.5b-ma} \sim 7''.3$, and $a_{\text{bar}}^{0.5r-ma} \sim 3''.6$. The final best estimated value will be provided in our H I 21 cm kinematical analysis presented in the following subsections.

3.1.2. VLA B-configuration H I 21 cm Gas Spatial Distribution

The optically thin H I 21 cm emission arises from cold atomic gas with an assumed spin temperature of $T_s \sim 100$ K or less (Field 1958a,b). Figure 5 shows the VLA B-configuration H I 21 cm integrated intensity over velocity (Moment 0) in both contours and grey scale. At the angular resolution of these VLA observations (synthesized beam FWHM $\sim 7''.1 \times 4''.2$) all the H I gas emission is within the optical disk of NGC 5597.

The comparison of the spatial distribution of the stars (blue and red optical images in Fig. 1 and Fig. 2), hot gas (H α , and cm radio continuum images, not shown here; Garcia-Barreto & Momjian 2022, in preparation)

and the cold H I gas (Fig. 5) in NGC 5597 seem to indicate that the H I clouds are at a slightly shorter radial distance than the few hot H II regions in the northern, eastern, south-east end, and western spiral arms. In other words, new star formation is taking place in the outer edges of the spiral arms. This is the expected spatial distribution per the density wave theory of spiral arms in disk galaxies. The alternative explanation for the total cold H I gas being a byproduct of photodissociation of H_2 regions might not seem to apply in the disk galaxy NGC 5597 (Allen 2002); there might be many photodissociation regions (PDRs) throughout the disk of NGC 5597, but they would be associated with localized star formation regions.

In NGC 5597, there are H II regions (hot gas) with no associated cold H I gas. One such example is the H I hole centered at $\alpha \sim 14^h 24^m 26^s.5$, $\delta \sim -16^\circ 46' 10''$, and another example is the innermost central (nucleus) region. In the innermost central region, there might exist cold dense molecular gas (H_2 , CO) where transitions from atomic to molecular gas are favored (Blitz & Rosolowsky 2006). While there does not seem to be yet any published CO observations for NGC 5597, one may expect $M_{H_2} \sim 6.4 \times 10^9 M_\odot$ from the CO - FIR correlation (Scoville 1988a) from its IRAS (FIR) luminosity $L_{\text{FIR}} \sim 2.2 \times 10^{10} L_\odot$. There are few examples in the literature on other nearby bright barred galaxies with molecular gas in their central re-

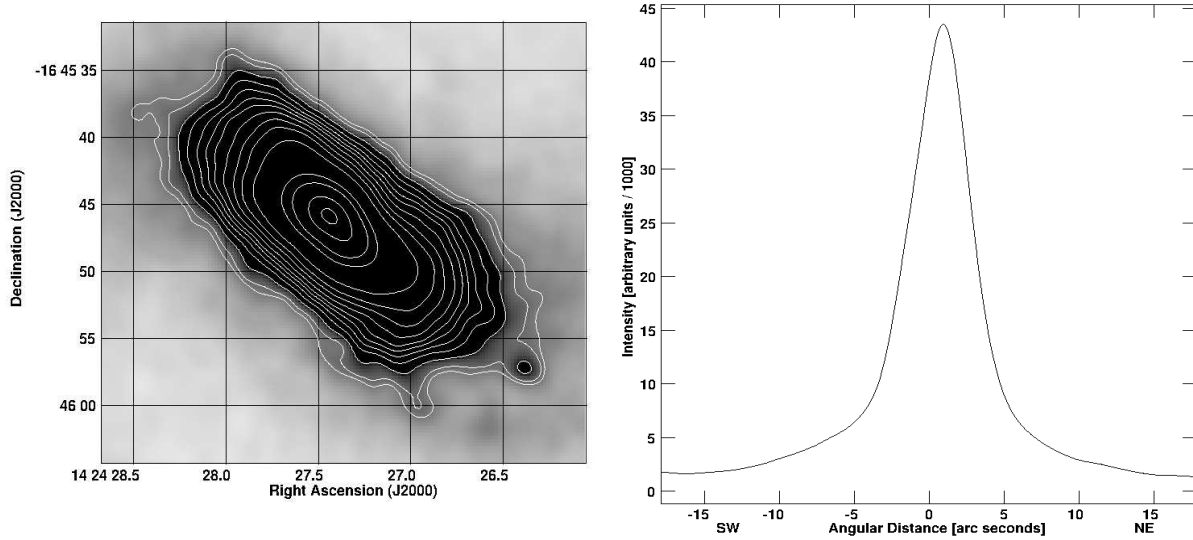


Figure 4. Left panel: innermost optical red, filter 8040 Å, continuum image of the stellar bar in NGC 5597 in grey scale and in contours, extracted from Figure 2 (Garcia-Barreto et al. 1996). The image had not been calibrated in intensity scale, thus the grey-scale stretch is in relative units proportional to noise from 2.8σ to 40σ , where $1\sigma = 45$ in arbitrary units, and the contours are at 34, 36, 40, 44, 48, 52, 56, 62, 70, 80, 100, 200, 300, 600 and $900 \times 1\sigma$, showing the extent of the boxy isophotal contours before a contour with azimuthal extensions. Box isophotes delineate a structure straddling the nucleus elongated in P.A. $\sim 52^\circ$ EofN. Right panel: one dimensional slice with intensity versus angular distance at P.A. $\sim 52^\circ$ EofN. Notice the lack of dust lanes.

gions, such as NGC 4314 (Combes et al. 1992), NGC 3367 (Garcia-Barreto et al. 2005, 2007), and NGC 1068 (Planesas, Scoville & Myers 1991). The innermost central region may also be the site of a nuclear bipolar outflow from a central supermassive black hole (SMBH), similar to what has been observed in the barred galaxies NGC 1068 (Wilson & Ulvestad 1987) and NGC 3367 (Garcia-Barreto et al. 1998, 2002), or the site of a nuclear bipolar geyser as in the barred galaxy NGC 1415 (Garcia-Barreto et al. 2019).

As for the south-west H I hole in NGC 5597 (and the H α image, not shown here, Garcia-Barreto & Momjian 2022 in preparation), it is at the approximate location of the anomalous SW spiral arm (labeled 2 in Fig. 2) with recent star formation and hot H II regions. In other external disk galaxies many cold H I gas holes have been detected where their large scale distribution is correlated with H II regions, suggesting that the H I holes are a result of intense OB star formation (i.e., M31) (Combes et al. 2002). It might also be a site of cold dense molecular gas (H_2 , CO), but there does not seem to be any published observations on NGC 5597 to support this.

The NGC 5597 - NGC 5595 disk galaxy pair is in an area of the universe with very low galaxy volume density (Tammann 1985; Tully & Fischer 1987), therefore, there is no hot intergalactic gas which could have stripped the atomic gas from outer disk radii. It seems

that both NGC 5595 and NGC 5597 originated with just enough primordial atomic neutral H I gas to form their disks and stars.

We note the narrow, curved, and long structures seen in H I emission in the NE with abrupt decrease in the emission toward the eastern side. Bright H I emission arises from the inner NE spiral arm in well correspondence with the optical arm. Somewhat weaker H I emission arises from the outer NE arm that seems to be at the inner edge of the optical eastern arm. The H I emission from the north arm is in the inner side of the optical continuum arm.

The outer northern optical spiral arm in NGC 5597 seen in Figures 1 and 2 (labeled 4 in Fig. 2), which indicates the spatial location of stars, is located at an approximate angular distance of $37'' \pm 5''$ from the nucleus (corresponding to a radial distance *on the plane of the sky* of about 6.9 ± 0.94 kpc). It is a well ordered, narrow, and curved structure seen from the north-west going counterclockwise to the north, north-east and east. The distance of the mean peak of its H I emission is about $30''.8 \pm 5''.8$ or at about 5.8 ± 1 kpc, and the far outer edge of the atomic gas emission ends abruptly at about 7.4 kpc. This spiral arm does not have a southern counterpart, however.

Since NGC 5597 has a disk companion, NGC 5595, to its north-west direction, a first possibility for the origin of the northern spiral arm might be a tidal grav-

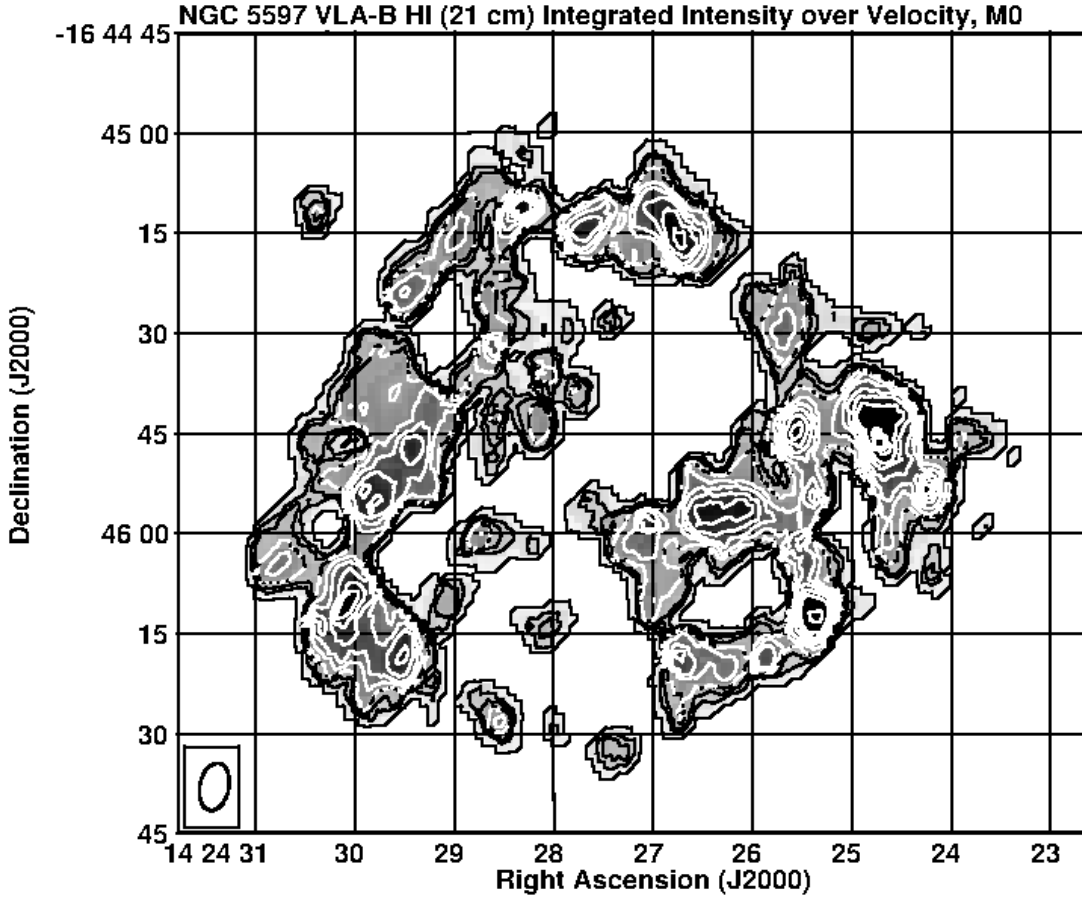


Figure 5. VLA B-configuration HI 21 cm integrated intensity over velocity, Moment 0, image of NGC 5597 in contours superposed on the same image in grey scale. Contours are 3, 35, 50, 70, 100, 125, 150, 175, 200, 250, 270 times $1\sigma \sim 0.3 \text{ mJy beam}^{-1} \text{ km s}^{-1}$. The grey scale ranges from 3σ to 200σ . The synthesized beam ($\sim 7''.1 \times 4''.2$ at FWHM) is shown in the lower left corner.

itational interaction (Combes et al. 2002); NGC 5597 might be in an early phase of a merger with NGC 5595 as studied by computer simulations in major mergers using a hierarchical tree method to calculate gravitational forces and smoothed particle hydrodynamics to follow the evolution of gas (Mihos & Hernquist 1996). A second possibility might be an $m=1$ gravitational instability as has been studied by self-gravitating computer simulations (Junquera & Combes 1996). An $m=1$ instability might be confined between the center of the galaxy and its Outer Lindblad Resonance (OLR) radius (Junquera & Combes 1996), however, an $m=1$ instability has been observed mainly on the gas distribution (and not on the star distribution; see Figures 5, 13, 17, and 19 in Junquera & Combes 1996). A third possibility might be the result of disk self evolution with or without gas accretion (Bournaud & Combes

2002), see for example their Figure 1 at 2.5 Gyrs, which roughly resembles the disk in NGC 5597. A fourth possibility would be the location near an OLR, where $\Omega_{\text{bar}} = \Omega_{\text{gas}} + \kappa/2$ (Sellwood & Wilkinson 1993; Buta & Combes 1996; Combes et al. 2002). A final fifth possibility would be the location of an outer $4/1$ ($m=4$) resonance (known as R1' type 1 OLR subclass outer pseudoring) where $\Omega_{\text{bar}} = \Omega_{\text{gas}} + \kappa/4$ between corotation and OLR (Sellwood & Wilkinson 1993; Buta & Combes 1996; Combes et al. 2002).

Our VLA HI emission results show a weak unresolved peak of cold gas at $\alpha \sim 14^{\text{h}} 24^{\text{m}} 28^{\text{s}}$, $\delta \sim -16^{\circ} 46' 15''$, as if it were the center of a circular area ($\sim 15''$ radius) devoid of HI gas. There is another area that lacks HI emission located to the SW of the optical stellar bar at $\alpha \sim 14^{\text{h}} 24^{\text{m}} 26^{\text{s}}.2$, $\delta \sim -16^{\circ} 46' 10''$. Furthermore, there is no atomic hydrogen cold gas emission from the posi-

tion of the optical nucleus at $\alpha(\text{J2000}) = 14^h 24^m 27^s.49$, $\delta(\text{J2000}) = -16^\circ 45' 45''.9$, nor from the circumnuclear region where there is hot gas ($T_e \sim 10^4 \text{ K}$; Spitzer 1978) as indicated by the $\text{H}\alpha$ emission (Garcia-Barreto et al. 1996) and the 20 cm radio continuum, most likely synchrotron, emission from that region (Condon et al. 1990; Garcia-Barreto & Momjian 2022 in preparation). There is also no H I 21 cm emission from the south-west optical disk in what seems to be a large elongated hole with an approximate size of $\sim 17'' \times 7''.5$ at P.A. $\sim 110^\circ$ EofN.

As a comparison, many other disk galaxies generally show H I 21 cm gas emission well beyond the optical disk [i.e., among them M83, SBc(s) II (Rogstad, et al. 1974), NGC 1300, SB(rs)bc (England 1989), NGC 3783, SBa, (Garcia-Barreto et al. 1999), NGC 3147 S(rs)bc (Haan et al. 2008), Maffei 2 SAB(rs)cd (Hurt, Turner & Ho 1996)]. In the case of gravitationally bound pairs, M51 is the best example with H I 21 cm cold gas emission from inner regions that follows the spiral structures, but it shows an extended broad tail to larger radii to the east of M51 with projected length of about 90 kpc (Rots, et al. 1990), while the M81 - M82 disk galaxy system, along with the small Irr II galaxy NGC 3077, shows H I 21 cm cold gas emission from an extensive array of filamentary tidal structures threading all three galaxies and indicating their interaction (Cottrell 1976; van der Hulst 1979; Yun, Ho & Lo 1994).

3.1.3. VLA B-configuration H I 21 cm Velocity Field and Kinematics

Our kinematical analysis was performed using the AIPS task *GAL*. After four iterations, it fitted the H I 21 cm parameters with the center at $\alpha(\text{J2000}) = 14^h 24^m 27^s.16$, $\delta(\text{J2000}) = -16^\circ 45' 46''.64$, which agrees well with the photometric coordinates of the nucleus (Diaz-Hernández et al. 2009), the position angle of the semi-major axis with redshifted velocities $\text{P.A.}_{\text{red HI}} \sim 100^\circ$ EofN, the inclination of the disk $i \sim 36^\circ$, and the systemic velocity $V_{\text{sys}} \sim 2698 \text{ km s}^{-1}$.

As noted above, the P.A. of the semi-major axis with redshifted velocities is $\sim 100^\circ$ EofN, with the corresponding P.A. of zero velocities compared to the systemic velocity (minor axis) at $\sim 10^\circ$ EofN⁶. Thus, the north-east, east, south hemisphere shows the redshifted

velocities while the north, north-west, west, south-west hemisphere shows the blueshifted velocities (figure of velocity field not shown, Garcia-Barreto & Momjian 2022 in preparation). Taking the P.A. $\sim 100^\circ$ EofN of the semi-major axis with redshifted velocities, and assuming the optical spiral arms are trailing, the hemisphere from north-west clockwise to south-east is closer to the observer. The orientation of the rotation axis vector points to the south-west at a projected P.A. $\sim 190^\circ$ EofN. This orientation will be important when analyzing the H I 21 cm gas kinematics and dynamics of both disk galaxies, NGC 5597 and NGC 5595, because the rotation axes are not parallel (Garcia-Barreto and Momjian 2022, in preparation).

Figure 6 shows our H I 21 cm VLA B-configuration spectrum of NGC 5597. The overall shape is very similar to the spectrum from the single dish radio telescope in Nançay which is the only one that has an appropriate east-west angular resolution ($\sim 3''.6$) to isolate the H I emission from NGC 5597 from that of NGC 5595 to the north-west (Paturel et al. 2003). The H I 21 cm spectra from other single dish radio telescopes, such as Parkes (64 m diameter) and Green Bank (91 m diameter), included the emission from both disk galaxies because their angular resolution was poor ($\sim 11''.5$ and $\sim 8''.1$, respectively) (Mathewson et al. 1992; Springob et al. 2005). Thus, neither the Parkes, nor the Green Bank observations, could show the individual spectra of the two galaxies, and they could not accurately estimate the systemic H I 21 cm velocity of either galaxy. The full widths of the H I line in NGC 5597 at 50% and 20% of the peak, obtained with the VLA in B-configuration, are $\Delta V_{50\%} \sim 211.40 \text{ km s}^{-1}$ and $\Delta V_{20\%} \sim 239.25 \text{ km s}^{-1}$, respectively (see Figure 6).

An explanation for the low flux density seen in the velocity interval from 2550 km s^{-1} to 2590 km s^{-1} is that it may be a plausible H I 21 cm emission from a weak but extended low surface density gas at the south-west of NGC 5597, perhaps as a tidal filamentary structure at $\alpha \approx 14^h 24^m 26''$, $\delta \approx -16^\circ 47'$ (Garcia-Barreto & Momjian 2022 in preparation).

In Figure 7, the left plot shows the fitted rotation curve with values slowly rising from $V \sim 24 \text{ km s}^{-1}$ at $R \sim 9''.23$ up to $V \sim 101 \text{ km s}^{-1}$ at $R \sim 61''.8$. The curve was obtained in confocal circular annuli each of them $8''.0$ wide, and integrated from $R = 0''.0 \rightarrow 70''.0$ with both hemispheres (Rogstad, et al. 1974). It shows a slowly rising curve, with a low velocity value near the central region. The right plot in Figure 7 shows the angular velocities of the H I gas assuming circular orbits: Ω_{gas} is shown by filled pentagons, $\Omega_{\text{gas}} - \kappa(R)/2$ is shown by

⁶ In a normal disk galaxy, in the approximation with only circular orbits ($v_R = 0, v_z = 0$) the velocity field will be symmetric about the minor axis with one side showing redshifted velocities compared to the galaxy's systemic velocity, and the other side showing blueshifted velocities (see Fig. 8-17 in Mihalas & Binney 1981).

open circles⁷, $\Omega_{\text{gas}} + \kappa(R)/2$ is shown by open triangles, and $\Omega_{\text{gas}} + \kappa(R)/4$ is shown by open squares. Ω_{gas} shows a low value at $R \sim 1.73$ kpc, then a high value at $R \sim 2.4$ kpc and then a (normal) decreasing curve which is less pronounced than a simple $\Omega_{\text{gas}} \propto 1/(R^{3/2})$, perhaps suggesting an extended central mass distribution⁸. The constant angular velocity corresponds to our estimated $\Omega_{\text{bar}} \sim 15.3 \text{ km s}^{-1} \text{ kpc}^{-1}$ assuming $\Omega_{\text{bar}} = \Omega_{\text{gas}}$ at corotation and $\mathcal{R} \equiv R_{\text{CR}}/a_{\text{bar}} = 1$. The constant value of Ω_{bar} crosses $\Omega_{\text{gas}} + \kappa/4$ at about a radius $R \sim 6.73$ kpc (see section 3.1.5 for the details on the interpretation).

3.1.4. VLA B-configuration: Total H I 21 cm Neutral Atomic Gas Mass in NGC 5597

The total integrated H I flux of NGC 5597 is $\int S_{\text{HI}} dv \sim 2.9 \text{ Jy km s}^{-1}$, measured using the task *IRING* in AIPS with concentric rings, each $8''.0$ wide, from $R = 0''.0 \rightarrow R = 80''.0$. The total estimated atomic hydrogen mass of NGC 5597 is $M(\text{H I}) \sim 1.02 \times 10^9 M_{\odot}$, which is very similar to e.g., the H I mass in Maffei 2 (Hurt, Turner & Ho 1996), a factor of 1.36 and 1.56 higher than the H I masses of M82 and NGC 3077, respectively, and which are both disk galaxies in a minor merger or in gravitational interaction, and is a factor of two lower than the H I mass in M81 (Yun, Ho & Lo 1994).

3.1.5. Corotation radius, R_{CR} , Angular Velocity Pattern Ω_{bar} , Outer Lindblad Resonance R_{OLR}

As mentioned previously in subsection 3.1.1, we have six different estimates for a_{bar} in NGC 5597 *on the plane of the sky* and *projected on the kinematical major axis of the disk (ma)*.

In this study, we think it would be more appropriate to analyze the six different estimates for the length of the stellar bar in NGC 5597 (a_{bar}) *projected on the ma of the disk* which are $a_{\text{bar}}^{d-ma} \sim 1.01$ kpc, $a_{\text{bar}}^{s-ma} \sim 1.74$ kpc, $a_{\text{bar}}^{blue-ma} \sim 1.87$ kpc, $a_{\text{bar}}^{red-ma} \sim 3.74$ kpc, $a_{\text{bar}}^{0.5b-ma} \sim 1.37$ kpc, and $a_{\text{bar}}^{0.5r-ma} \sim 0.67$ kpc.

Since we utilize the resonance method to estimate the angular velocity of the stellar bar, Ω_{bar} , in NGC 5597 assuming that the corotation radius lies at the end of the bar's length, we proceed now to consider the different estimates of a_{bar} in combination with the kinematical H I data, i.e., rotation curve and angular velocities (Figure 7), to estimate the radii of the outer $m = 2$ and $m = 4$ resonances.

⁷ $\kappa(R)$ is the small radial motion of gas due to the non-axisymmetrical gravitational potential of a stellar bar. It may be estimated from the expression $\kappa(R) = \sqrt{4\Omega_{\text{gas}}^2 + 2R\Omega_{\text{gas}}(d\Omega_{\text{gas}}/dR)}$

⁸ Modeling a detailed mass distribution in NGC 5597 is beyond the scope of the present study.

This method has been proven to be valid when applied to nearby bright galaxies with ring structures near the ILR and the OLR (Binney & Tremaine 1987; Combes 1988; Sellwood & Wilkinson 1993; Buta & Combes 1996; Elmegreen 1996a; Elmegreen et al. 1996b). Assuming that the end of the boxy stellar bar is the radius of corotation, R_{CR} (Contopoulos 1980; Contopoulos & Papayannopoulos 1980; Contopoulos 1981), that is, $\mathcal{R} \equiv R_{\text{CR}}/a_{\text{bar}} = 1$, the resonance method, with an epicycle frequency $\kappa(R)$, indicates that at this radius $\Omega_{\text{gas}} = \Omega_{\text{bar}}$.

From the angular rotation curve (Figure 7–Right), we are obliged only to consider values for a_{bar} (projected on the kinematical major axis of the disk) larger than 1.73 kpc ($9''.23$) because our observations did not detect any H I 21 cm gas at smaller radii. Thus, we are left with only three possible values, namely, $a_{\text{bar}}^{s-ma} \sim 1.74$ kpc, $a_{\text{bar}}^{blue-ma} \sim 1.87$ kpc, and $a_{\text{bar}}^{red-ma} \sim 3.74$ kpc.

First, if $a_{\text{bar}}^{s-ma} \sim 1.74$ kpc ($\sim 9''.3$) were the corotation radius, then it would result in Ω_{gas} at an anomalous low value of $\sim 13.8 \text{ km s}^{-1} \text{ kpc}^{-1}$ and it would set $\Omega_{\text{bar}} = \Omega_{\text{gas}}$ at that constant value that is well above the values of $\Omega_{\text{gas}} - \kappa(R)/2$. This constant value of Ω_{bar} crosses $\Omega_{\text{bar}} \sim \Omega_{\text{gas}} + \kappa(R)/4$ at a radius $R_{\text{Om}=4} \sim 9.8$ kpc, and $\Omega_{\text{bar}} \sim \Omega_{\text{gas}} + \kappa(R)/2$ at a radius $R_{\text{OLR}} \sim 11.50$ kpc.

Second, if $a_{\text{bar}}^{b-ma} \sim 1.87$ kpc ($\sim 10''$) were the corotation radius, then it would indicate Ω_{gas} at an anomalous low value $\sim 14.8 \text{ km s}^{-1} \text{ kpc}^{-1}$ and it would set $\Omega_{\text{bar}} = \Omega_{\text{gas}}$ at that constant value that is also well above the values of $\Omega_{\text{gas}} - \kappa(R)/2$. This constant value of Ω_{bar} will cross $\Omega_{\text{gas}} + \kappa(R)/4$ at a radius $R_{\text{Om}=4} \sim 6.96$ kpc, and $\Omega_{\text{bar}} \sim \Omega_{\text{gas}} + \kappa(R)/2$ at a radius $R_{\text{OLR}} \sim 11.37$ kpc.

Finally, taking $a_{\text{bar}}^{r-ma} \sim 3.74$ kpc ($\sim 20''$) as the corotation radius, it would result in $\Omega_{\text{gas}} \sim 15.3 \text{ km s}^{-1} \text{ kpc}^{-1}$. It would then set $\Omega_{\text{bar}} = \Omega_{\text{gas}}$ at that constant value that is also well above the values of $\Omega_{\text{gas}} - \kappa(R)/2$. This constant value of Ω_{bar} will cross $\Omega_{\text{gas}} + \kappa(R)/4$ at a radius $R_{\text{Om}=4} \sim 6.73$ kpc, and $\Omega_{\text{bar}} \sim \Omega_{\text{gas}} + \kappa(R)/2$ at a radius $R_{\text{OLR}} \sim 11.25$ kpc.

Considering a) the extent, or the distance projected on the kinematical major axis of the galaxy, of the red optical boxy isophotal contours (Figures 2 and 4) before the next isophotal contour that starts to extend azimuthally ($a_{\text{bar}}^{r-ma} \sim 20''$, or $a_{\text{bar}}^{r-ma} \sim 3.74$ kpc), b) the distance from the center to the mean optical red northern arm ($R_{\text{red}}^{nnw} \sim 6.7$ kpc), c) the rotation curve and angular velocities from our H I 21 cm results, and d) $\mathcal{R} \equiv R_{\text{CR}}/a_{\text{bar}} = 1$, then our best estimate for Ω_{bar} of the stellar bar in NGC 5597 with the resonance method is $\Omega_{\text{bar}} \sim 15.3 \text{ km s}^{-1} \text{ kpc}^{-1}$.

How does this value of $\Omega_{\text{bar}}^{\text{NGC5597}}$ compare with those obtained for other galaxies? Excellent observational

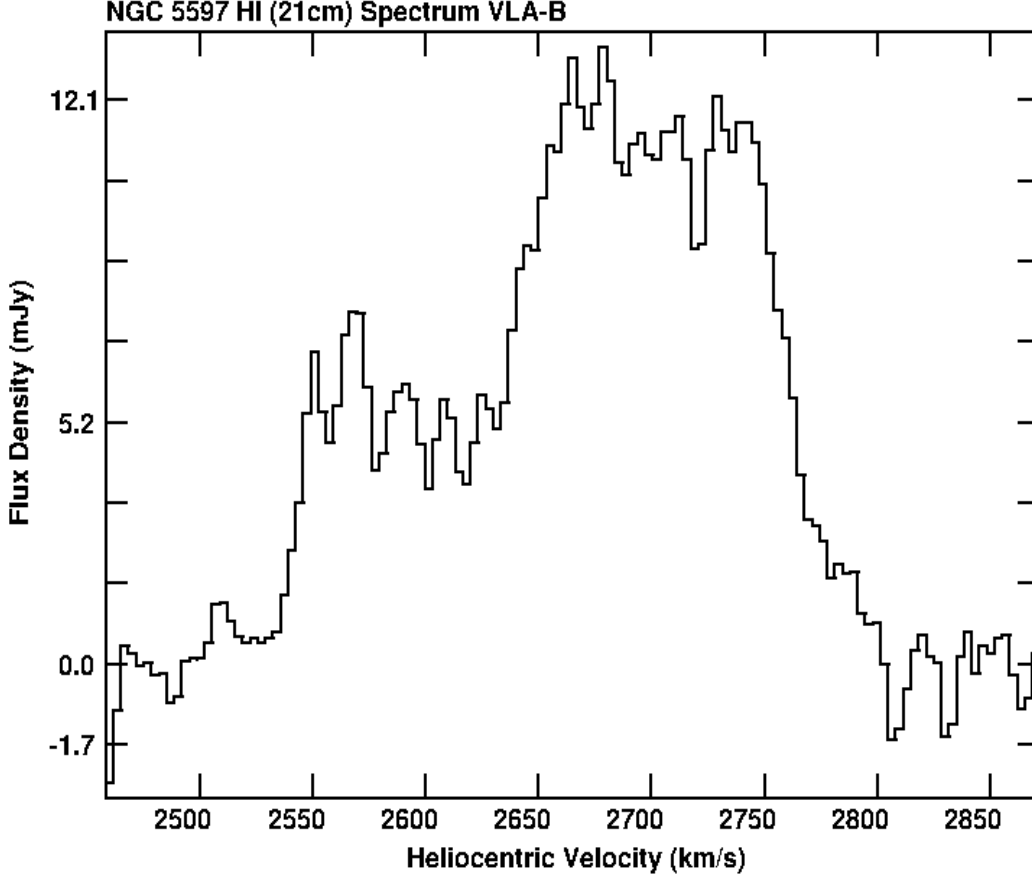


Figure 6. VLA B-configuration H I 21 cm spectrum of NGC 5597. The heliocentric systemic velocity, fitted by the task *GAL* in AIPS, is $V_{\text{sys-helio}} = 2698 \text{ km s}^{-1}$, and the widths at 50% and 20% of the peak are $\Delta V_{50\%} \sim 211.40 \text{ km s}^{-1}$ and $\Delta V_{20\%} \sim 239.25 \text{ km s}^{-1}$, respectively. Comparing the flux density scale to previous Parkes (64 m) and Green Bank (91m) single dish radio telescope spectra is very difficult because their beams included both disk galaxies NGC 5595 and NGC 5597 (Mathewson et al. 1992; Springob et al. 2005). The shape of the VLA spectrum looks very similar to that of Nancay’s, which has an elongated beam of ~ 3.6 east-west \times $22'$ north-south at FWHM (Paturel et al. 2003).

studies have estimated Ω_{bar} for two barred galaxies: NGC 936 and NGC 4596. For NGC 936, $\Omega_{\text{bar}}^{\text{NGC936}} \sim 60 \pm 14 \text{ km s}^{-1} \text{ kpc}^{-1}$ (Merrifield & Kuijken 1995) derived from the velocity field of stars using the Tremaine-Weinberg (TW) method (Tremaine & Weinberg 1984), $38 \leq \Omega_{\text{bar}}^{\text{NGC936}} \leq 64 \text{ km s}^{-1} \text{ kpc}^{-1}$ (Kent & Glaudell 1989), and $\Omega_{\text{bar}}^{\text{NGC936}} \sim 71 \text{ km s}^{-1} \text{ kpc}^{-1}$ (Kormendy 1983).

If we re-do the previously published analysis taking a) $a_{\text{bar}}^{\text{NGC936}} \sim 51''$ projected on the kinematical major axis of the galaxy, which translates to $a_{\text{bar}}^{\text{NGC936}} \sim 3.96 \text{ kpc}$ (Kormendy 1983; Kent & Glaudell 1989; Kent 1990), b) $R_{\text{CR}}^{\text{NGC936}} \sim 4.1 \text{ kpc}$ (Kormendy 1983), c) a lower limit value of $\Omega_{\text{bar}}^{\text{NGC936}} \sim 46 \text{ km s}^{-1} \text{ kpc}^{-1}$ (Merrifield & Kuijken 1995), then it would set $\mathcal{R} \equiv R_{\text{CR}}/a_{\text{bar}} \sim 0.96$ (a value very close to 1).

For NGC 4596, the values are $\Omega_{\text{bar}}^{\text{NGC4596}} \sim 52 \pm 13 \text{ km s}^{-1} \text{ kpc}^{-1}$ (Gersen, Kuijken & Merrifield 1999) using the TW method, and $\Omega_{\text{bar}}^{\text{NGC4596}} \sim 43 \text{ km s}^{-1} \text{ kpc}^{-1}$

(Kent 1990). Also, there are two values reported for a_{bar} , the first $a_{\text{bar}}^{\text{NGC4596}} \sim 75''$ projected on the kinematical major axis of the galaxy, or $a_{\text{bar}}^{\text{NGC4596}} \sim 5.7 \text{ kpc}$ (Kormendy 1979), and the second $a_{\text{bar}}^{\text{NGC4596}} \sim 66''$ the radius where the intensity has fallen to half of its peak value along the bar’s major axis, or $a_{\text{bar}}^{\text{NGC4596}} \sim 5 \text{ kpc}$, (Kent 1990). Additionally $R_{\text{CR}}^{\text{NGC4596}} \sim 6.3 \text{ kpc}$ (Kent 1990). Similarly, if we re-do the analysis for NGC 4596, taking a) the lower limit value of $\Omega_{\text{bar}}^{\text{NGC4596}} \sim 39 \text{ km s}^{-1} \text{ kpc}^{-1}$ (Gersen, Kuijken & Merrifield 1999; Kent 1990), b) $a_{\text{bar}}^{\text{NGC4596}}$ from Kormendy (1979), then it would suggest $\mathcal{R} \equiv R_{\text{CR}}/a_{\text{bar}} \sim 1$. If one were to take the upper limit value of $\Omega_{\text{bar}}^{\text{NGC4596}} \sim 65 \text{ km s}^{-1} \text{ kpc}^{-1}$

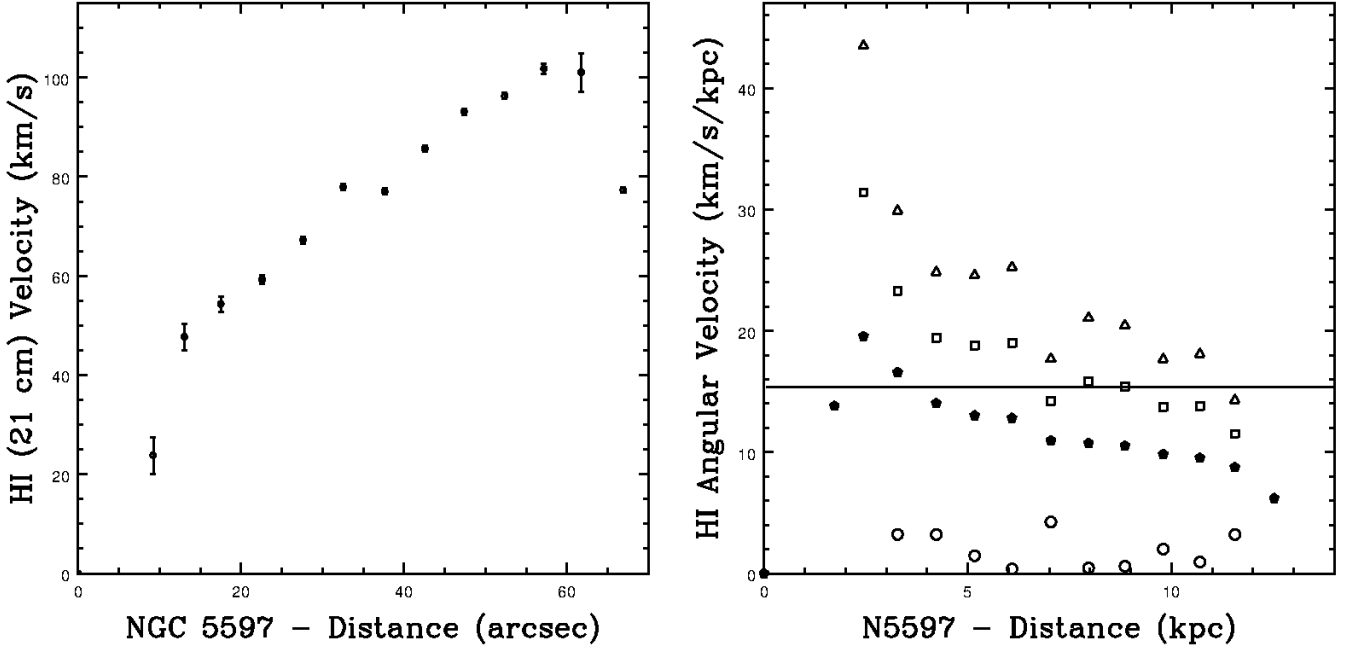


Figure 7. *Left:* VLA B-configuration H I 21 cm rotation curve of NGC 5597 after several iterations utilizing the task *GAL* in AIPS. The final fitted systemic heliocentric velocity is $V_{\text{sys-helio}} = 2698 \text{ km s}^{-1}$. *Right:* The angular velocity of the H I 21 cm gas, Ω_{gas} (filled pentagons), $\Omega_{\text{gas}} - \kappa(R)/2$ (open circles), $\Omega_{\text{gas}} + \kappa(R)/2$ (open triangles), $\Omega_{\text{gas}} + \kappa(R)/4$ (open squares), where $\kappa(R)$ is the epicycle frequency. The angular velocity pattern of a stellar bar, Ω_{bar} , is equal to the angular velocity of the gas, Ω_{gas} , in the epicycle approximation at corotation. Our estimation of $a_{\text{bar}}^{r-ma} \sim 20''$ ($\sim 3.74 \text{ kpc}$) in NGC 5597 (see Section 3.1.5) as the corotation radius would result in $\Omega_{\text{gas}} \sim 15.3 \text{ km s}^{-1} \text{ kpc}^{-1}$, therefore $\Omega_{\text{bar}} \sim 15.3 \text{ km s}^{-1} \text{ kpc}^{-1}$ (the constant horizontal line). This Ω_{bar} value crosses $\Omega_{\text{gas}} + \kappa(R)/4$ at a radius $R_{\text{Om}=4} \sim 6.73 \text{ kpc}$, and $\Omega_{\text{gas}} + \kappa(R)/2$ at a radius $R_{\text{OLR}} \sim 11.25 \text{ kpc}$

(Gersen, Kuijken & Merrifield 1999; Kent 1990) then it would suggest $\mathcal{R} \equiv R_{\text{CR}}/a_{\text{bar}} \sim 1.1^9$.

Therefore, we believe that our assumption of $\mathcal{R} \equiv R_{\text{CR}}/a_{\text{bar}} \sim 1$ is reasonable, and our value of Ω_{bar} in NGC 5597 SBc(s), estimated using the resonance method, is similar or a bit smaller than the values for other bright and nearby barred galaxies, i.e., $\Omega_{\text{bar}} \sim 60 \text{ km s}^{-1} \text{ kpc}^{-1}$ in NGC 1326 (RSBa with a circumnuclear ring) (Garcia-Barreto et al. 1991b), $\Omega_{\text{bar}} \sim 134 \text{ km s}^{-1} \text{ kpc}^{-1}$ in NGC 1415 (SBa with a geyser or low velocity bipolar nuclear H α outflow) (Garcia-Barreto et al. 2019), $\Omega_{\text{bar}} \sim 39 - 43 \text{ km s}^{-1} \text{ kpc}^{-1}$ in NGC 3367 (SBc compact nuclear ring and radio bipolar outflow) (Garcia-Barreto & Rosado 2001; Garrido-Roman 2014), $\Omega_{\text{bar}} \sim 38 \text{ km s}^{-1} \text{ kpc}^{-1}$ in NGC 3783 (SBa Seyfert 1 and strong X-ray emission and X-ray variability) (Garcia-Barreto et al. 1999), and

$\Omega_{\text{bar}} \sim 36 \text{ km s}^{-1} \text{ kpc}^{-1}$ in NGC 4314 (SBa(rs)p with a circumnuclear ring) (Garcia-Barreto et al. 1991a).

Lastly, from the right plot in Figure 7, Ω_{bar} crosses $\Omega_{\text{gas}} + \kappa(R)/4$ at a radius, $R \sim 6.73 \text{ kpc}$; this radius corresponds to the spatial location of the north optical spiral arm structure seen in Figures 1 and 2. From our H I 21 cm VLA B-configuration kinematical observations we cannot estimate any radius for a plausible ILR. Furthermore, our observations combined with the resonance method and $\mathcal{R} = 1$ suggests that a plausible interpretation for the north spiral optical arm might be an outer m=4 resonance in NGC 5597 (Contopoulos et al. 1989; Athanassoula 1992).

4. SUMMARY AND CONCLUSIONS

In this study, we have obtained VLA B-configuration H I 21 cm kinematical data from the disk galaxy NGC 5597 SBc(s). We were able to obtain the two dimensional velocity field and to estimate the *best fit* rotation curve assuming the neutral gas is in circular orbits around the nucleus. From the rotation curve of NGC 5597, we have calculated Ω_{gas} , $\kappa(R)$, $\Omega_{\text{gas}} - \kappa(R)/2$, $\Omega_{\text{gas}} + \kappa(R)/2$ and $\Omega_{\text{gas}} + \kappa(R)/4$.

⁹ If, however, one were to take $a_{\text{bar}}^{\text{NGC4596}}$ from Kent (1990) together with the lower limit value of $\Omega_{\text{bar}} \sim 39 \text{ km s}^{-1} \text{ kpc}^{-1}$ (Gersen, Kuijken & Merrifield 1999), then it would suggest $\mathcal{R} \equiv R_{\text{CR}}/a_{\text{bar}} \sim 1.15$, and if one were to take the upper limit value $\Omega_{\text{bar}} \sim 65 \text{ km s}^{-1} \text{ kpc}^{-1}$ (Gersen, Kuijken & Merrifield 1999) then it would suggest $\mathcal{R} \equiv R_{\text{CR}}/a_{\text{bar}} \sim 1.26$

From our previously published studies, we have our best estimate for a_{bar} as $a_{\text{bar}}^{r-ma} \sim 20''$ projected on the kinematical major axis of the H I cm in the disk, or $a_{\text{bar}} \sim 3.74$ kpc.

We have assumed that the radius at which corotation occurs, R_{CR} , is just at the end of the semimajor axis of the stellar bar in NGC 5597, $\mathcal{R} \equiv R_{\text{CR}}/a_{\text{bar}} = 1$ (Contopoulos 1980; Contopoulos & Papayannopoulos 1980; Kormendy 1983). With this assumption and the angular velocities, we estimated the angular velocity for the stellar bar in NGC 5597 to be $\Omega_{\text{bar}} \sim 15.3 \text{ km s}^{-1} \text{ kpc}^{-1}$. Additionally, this constant value of

Ω_{bar} crosses the curve $\Omega_{\text{gas}} + \kappa(R)/4$ at 6.73 kpc, which is very similar to the radius of the spatial location of the optical north spiral arm in NGC 5597. Therefore, we have interpreted this as an outer m=4 resonance arm.

We thank the anonymous referee for suggestions and comments that have significantly enhanced the content of this manuscript.

Facilities: EVLA

Software: AIPS: (Greisen 2003), CASA (McMullin et al. 2007)

REFERENCES

- Allen, R. J., 2002, Dynamics, Structure & History of Galaxies, ASP Conf.S., 273, 183, Ed. G.S. Da Costa & H. Jersén
- Athanassoula, E., 1992, MNRAS, 259, 345
- Athanassoula, E., 2003, MNRAS, 341, 1179
- Athanassoula, E., & Misiriotis, A., 2002, MNRAS, 330, 35
- Binney, J., & Tremaine, S. 1987 Galactic Dynamics (Princeton: Princeton Univ. Press)
- Blitz, L., & Rosolowsky, E., ApJ, 650, 933
- Bournaud, F., & Combes, F. 2002, A&A, 392, 83
- Buta, R., & Combes, F., 1996, Fund.Cosmic Physics, 17, 95
- Cecil, G. 1988, ApJ, 329, 38
- Combes, F. 1988, in *Galactic and Extragalactic Star Formation*, eds. Ralph E. Pudritz, & M. Fich, NATO ASI, Series C, 232, p. 475 (Dordrecht: Kluwer Academic Publ.)
- Combes, F., Boissé, P., Mazure, A. & Blanchard, A. 2002, *Galaxies and Cosmology*, (Berlin: Springer-Verlag)
- Combes, F., Gerin, M., Nakai, N., Kawabe, R. & Shaw, M.A., 1992, A&A, 259, L27
- Condon, J.J., Helou, G., Sanders, D.B., & Soifer, B.T. 1990, ApJS, 73, 359
- Contopoulos, G., 1980, A&A, 81, 198
- Contopoulos, G., Gottesman, S.T., Hunter, J.H.Jr., & England, M.N. 1989, ApJ, 343, 608
- Contopoulos, G., & Papayannopoulos, Th. 1980, A&A, 92, 33
- Contopoulos, G., 1981, A&A, 102, 265
- Cottrell, G. A., 1976, MNRAS, 174, 455
- Crane, P., & van der Hulst, J., M., 1992, AJ, 103, 1146
- Dedattista, V.P. & Sellwood, J. A., 2000, ApJ, 543, 721
- Diaz-Garcia, S., Salo, H., Laurikainen, E., & Herrera-Endoqui, M. 2016, A&A, 587, 160
- Diaz-Hernández, R., Garcia-Barreto, J.A., & Moreno-Corral, M. A., 2009, Rev.Mex.Fis., E55, 70
- Elmegreen, B. G., 1996a, ASP. Conf.S., 91,197
- Elmegreen, B. G., Elmegreen, D. M., Chromey, F. R., Hasselbacher, D. A., & Bissell, B. A. 1996b, AJ, 111, 2233
- England, M. N. 1989, ApJ, 337, 191
- Erwin, P. 2005, MNRAS, 283, 302
- Field, G.F. 1958a, Proc. I.R.E., 46, 240
- Field, G.F. 1958b, ApJ, 129, 536
- Ford, H.C., Crane, P.C., Jacoby, G.H., Lawrie, D.G., & van der Hulst, J.M. 1985, ApJ, 293, 132
- Garcia-Barreto, J. A., Downes, D., Combes, F., Gerin, M., Magri, C., Carrasco, L. & Cruz-Gonzalez, I. 1991a, A&A, 244, 257
- Garcia-Barreto, J. A., Dettmar, R.J., Combes, F., Gerin, M. & Koribalski, B., 1991b, RMxAA, 22, 197
- Garcia-Barreto, J. A., Combes, F., Koribalski, B. & Franco, J. 1999, A&A, 348, 685
- Garcia-Barreto, J.A., Franco, F., Carrillo, R., Venegas, S. & Escalante-Ramirez, B. 1996, RMxAA, 32, 89
- Garcia-Barreto, J. A., Franco, J., & Rudnick, L. 2002, AJ, 123, 1913
- Garcia-Barreto, J.A., Mayya, D.Y., & Guichard, J. 2019, PASP, 131:094101
- Garcia-Barreto, J. A., & Rosado, M. 2001, AJ, 121, 2540
- Garcia-Barreto, J.A., Rudnick, L., Franco, F., & Martos, M. 1998, AJ, 116, 111
- Garcia-Barreto, J. A., Scoville, N.Z., Koda, J. & Sheth, K. 2005, AJ, 129, 125
- Garcia-Barreto, J. A., Scoville, N.Z., Koda, J. & Sheth, K. 2007, Triggering Relativistic Jets RMxAA, Conf.S., 27, 258
- Garrido-Roman, R.E. 2014, BSc Thesis, School of Sciences, UNAM (Mexico City)

- Gersen, J., Kuijken, K. & Merrifield M.R. 1999, MNRAS, 306, 926.
- Goad, J. W. 1976, ApJS, 32, 89
- Greisen, E. W. 2003, Information Handling in Astronomy - Historical Vistas, 285, 109
- Haan, S., Schinnerer, E., Mundell, C.G., Garcia-Burillo, S., & Combes, F. 2008, AJ, 135, 232
- Hurt, R.L., Turner, J. L., & Ho, P.T.P. 1996, ApJ, 466, 135
- Junqueira, S. & Combes, F. 1996, A&A, 312, 703
- Kent, S. M. 1990, AJ, 100, 377
- Kent, S. M. & Glaudell, G. 1989, AJ, 98, 1588
- Kormendy, J. 1977, ApJ, 214, 359
- Kormendy, J. 1979, ApJ, 227, 714
- Kormendy, J. 1983, ApJ, 275, 529
- Lynden-Bell, D. 1979, MNRAS, 187, 101
- Lynden-Bell, D., & Kalnajs, A.J. 1972, MNRAS, 157, 1
- Martin, P. 1995, AJ, 109, 2428
- Mathewson, D.S., Ford, V. L. & Buchhorn M. 1992, ApJS, 81, 413
- McMullin, J. P., Waters, B., Schiebel, D., Young, W., & Golap, K. 2007, in Astronomical Society of the Pacific Conference Series, Vol. 376, Astronomical Data Analysis Software and Systems XVI, ed. R. A. Shaw, F. Hill, & D. J. Bell, 127
- Merrifield M.R., & Kuijken, K. 1995, MNRAS, 274, 933.
- Mihalas, D., & Binney, J., 1981, *Galactic Astronomy* (2nd. Ed. San Francisco: Freeman)
- Mihos, J.C., & Hernquist, L. 1996, ApJ, 464, 641
- Moody, J. W., Roming, P. W. A., Joner, M. D., Hintz, E. G., Geisler, D., Durrell, P. R., Scowen, P. A., & Jee, R. O. 1995, AJ, 110, 2088
- Norman, G., & Silk, J., 1983, ApJ, 266, 502.
- Paturel, G., Thereau, G., Bottinelli, L., Gouguenheim, L., Coudreau-Durand, N. Hallet, N. & Petit, C. 2003, A&A, 412, 57
- Planesas, P., Scoville, N.Z., & Myers, S. T. 1991, ApJ, 369, 364
- Quillen, A.C., Frogel, J.A., & Gonzalez, R.A. 1994, ApJ, 437, 162
- Rogstad, D.H., Lockhart, I.A. & Wright, M.C.H. 1974, ApJ, 193, 309
- Rots, A.H., Bosma, A., van der Hulst, J.M., Athanassoula, E. & Crane, P.C. 1990, AJ, 100, 387
- Salo, H., Laurikainen, E., Laine, J., Comerón, S., + 20 authors, 2015, ApJS, 219:4, July
- Sandage, A., & Tammann, G.A., 1987, A Revised Shapley-Ames Catalog of Bright Galaxies (Washington, DC: Carnegie Institution of Washington)
- Scoville, N. Z. 1988, *Galactic and Extragalactic Star Formation* (Dordrecht: Kluwer Academic Publishers, Nato ASI Series 232, p. 541)
- Scoville, N. Z., Matthews, K., Carico, D.P., & Sanders, D.B., 1988, ApJ, 327, L61
- Scoville, N. Z., Yun, M. S., Armus, L., & Ford, H. 1998, ApJ, 493, L63
- Sellwood, J.A., & Wilkinson, A. 1993, Rep.Prog.Phys, 56, 173
- Spitzer, L. Jr., 1978, Physical Processes in the Interstellar Medium (New York: John Wiley & Sons)
- Springob, C. M., Haynes, M. P., Giovanelli, R., & Kent, B. R. 2005, ApJS, 160, 149
- Tammann, G. A. 1985 ESO Conf. Proc., 20 *The Virgo Cluster of Galaxies*, Eds. O.-G. Richter & B. Binggeli (Garching: ESO)
- Tremaine, S., & Weinberg, M. D. 1984, ApJ, 282, L5
- Tully, R.B. 1988 Nearby Galaxies Catalog, (Cambridge: Cambridge Univ. Press)
- Tully, R.B. & Fischer, J. R. 1987 Nearby Galaxies Atlas, (Cambridge: Cambridge Univ. Press)
- Ulvestad, J.S.; Neff, S. G. & Wilson, A. S. 1987, AJ, 93, 22
- van der Hulst, J., M. 1979, A&A, 75, 97
- Veilleux, S., Cecil, G., Bland-Hawthorn, J., Tully, R. B., Filippenko, A., V., & Sargent, W. L. W. 1994, ApJ, 433, 48
- Wilson, A.S. & Ulvestad, J.S. 1987, ApJ, 319, 105
- Yun, M.S., Ho, P.T.P. & Lo, K. Y. 1994, Nature, 372, 530.